Zamudio-Ramirez, I.; Antonino-Daviu. J.; Osornio-Rios, RA.; Dunai, L. (2022). Tracking of high-order stray-flux harmonics under starting for the detection of winding asymmetries in wound-rotor induction motors. IEEE Transactions on Industrial Electronics. 69(8):8463-8471. https://doi.org/10.1109/TIE.2021.3108716

Tracking of high-order stray-flux harmonics under starting for the detection of winding asymmetries in wound-rotor induction motors

Israel Zamudio-Ramirez, Jose A. Antonino-Daviu, *IEEE Senior Member*, Roque A. Osornio-Rios, *IEEE Senior Member,* and Larisa Dunai, *IEEE Member*

***Abstract*— Wound rotor induction motors (WRIM) are widely used in a vast number of high output power industrial applications due to their capability of reaching high start torques while maintaining low inrush currents. Nonetheless, these machines are very prone to require early maintenance, and the possibility of presenting rotor winding asymmetry failures is high due to their more complex rotor circuit. Although some recent works have proposed techniques that overcome the drawbacks of conventional methods, an additional research effort for the development of alternative approaches able to enhance their performance and reliability is desirable. In this work, a new method for the diagnosis of rotor asymmetries in WRIM is presented. The proposed methodology is based on a feed-forward neural network (FFNN) feed by suitable fault severity indicators, which rely on the maximum energy density of higher order harmonics (amplified by the failure) at strategic regions of the time-frequency maps obtained from stray flux signals under startup transient. Experimental results for three different levels of rotor asymmetries in a 11 KW WRIM prove the reliability of the enhanced proposed system in comparison to conventional approaches that only rely on the main sideband fault-harmonic amplitudes.**

***Index Terms*— wound rotor induction motors, fault diagnosis, rotor asymmetries, transient analysis, stray flux, currents.**

I. Introduction

WOUND rotor induction motors (WRIM) are much less used in industry than their cage counterparts. Their greater constructive complexity together with their frequent maintenance problems make the use of cage induction motors preferable, compared to the use of WRIM [1], [2]. Nonetheless, these motors also have important advantages that make them a very interesting option in many applications of diverse industries (cement, paper, steel, water distribution, etc.). One of these advantages is the possibility of accessing the rotor winding, which enables the insertion of external rheostats during motor starting; this modifies the torque-speed characteristic of these machines, yielding higher starting torques, while maintaining low starting currents [3]. This advantage is crucial when starting loads that present high resistive torques. It is frequent to find this type of motors in the medium-high power range (usually, above 1,000 hp), driving loads such as pumps, cranes, fans, ball and sag mills, lowers or conveyors [2]. In the past, these machines were also a preferred alternative for variable speed applications, taking part in configurations as the Subsynchronous Cascade Drive (SCD), which is also widely known as Slip Energy Recovery Drive (SERD) [4].

Despite their wide use in specific industrial applications, WRIM are very prone to require early maintenance and different faults may take place in a WRIM. Among them, rotor winding asymmetries are rather frequent. This is mainly due to their more complex rotor circuit, which is not only based on the

Manuscript received Month xx, 2xxx; revised Month xx, xxxx; accepted Month x, xxxx. This work was supported by the Spanish 'Ministerio de Ciencia Innovación y Universidades' and FEDER program in the framework of the 'Proyectos de I+D de Generación de Conocimiento del Programa Estatal de Generación de Conocimiento y Fortalecimiento Científico y Tecnológico del Sistema de I+D+i, Subprograma Estatal de Generación de Conocimiento' (ref: PGC2018-095747-B-I00).

Israel Zamudio-Ramirez is with CA Mecatronica, Facultad de Ingenieria, Campus San Juan del Rio, Universidad Autonoma de Queretaro, San Juan del Rio 76807, Queretaro, MEXICO and with Department Electrical Engineering, Universitat Politècnica de València, Camino de Vera s/n, 46022, Valencia, SPAIN (e-mail: isra.zam.ram@hotmail.com).

Jose Antonino-Daviu is with the Instituto Tecnologico de la Energia, Universitat Politècnica de València, Camino de Vera s/n, 46022, Valencia, SPAIN (e-mail: joanda@die.upv.es).

Roque A. Osornio-Rios is with CA Mecatronica, Facultad de Ingenieria, Campus San Juan del Rio, Universidad Autonoma de Queretaro, San Juan del Rio 76807, Queretaro, MEXICO (e-mail: raosornio@hspdigital.org).

Larisa Dunai is with the Centro de Investigación en Tecnologías Gráficas, Universitat Politècnica de València, Camino de Vera s/n, 46022, Valencia, SPAIN (e-mail: ladu@upv.es).

winding itself, but also on additional elements such as slip rings/brushes system, external rheostat, as well as the different switchgear and connections between all these elements. The conclusion is that an asymmetry in the rotor circuit may be created by problems in any of these components, a fact that yields a high number of potential sources for this failure: uneven wear of brushes, defective contacts between slip and brushes, high resistance connections between coils of the rotor winding, unbalances in the external rheostat, among others. In this context, some predictive maintenance techniques such as current analysis or even infrared thermography have been developed for detecting rotor asymmetry problems in WRIM [5]–[7]. The conventional Motor Current Signature Analysis (MCSA) is currently the most widespread online approach in industry for detecting asymmetries in WRIM. This is mainly due to its remote capability to assess the machine condition from the motor control center. However, MCSA exhibits well-known problems, especially those related to its intrinsic implications (i.e., non-suitable for non-stationary signals, potential false indications caused by constructive characteristics or operating conditions of the machine, etc.). This has encouraged some authors to search for alternative methods that could enhance the diagnosis of rotor winding faults in WRIM. In this regard, novel techniques based on the analysis of the current demanded by the motor under starting were proposed [5], showing that the identification of the patterns created by the fault components under that transient by using appropriate time-frequency (t-f) tools is a suitable method to diagnose the presence of the asymmetry. Despite the efforts toward the enhancement of current-based methodologies, well-known drawbacks of such methods have recently been pointed out. For example, in [8] it is demonstrated that low frequency load oscillations are transferred through the coupling and reflected in the current spectrum as low frequency sidebands of the power supply frequency (f). In [9], it is shown that eccentricity faults produce equivalent frequency components as asymmetries in WRIM with high amplitudes in the main sideband harmonics. Furthermore, eccentricity/misalignment components and components related to load malfunction are not well discriminated via current analysis [10]. Evidently, main sideband harmonics of current signals may lead to potential false diagnosis. In this regard, more recently, researchers have proposed the use of stray-flux based techniques (under steady-state and under starting) for the detection of rotor winding asymmetries [11], [12]. As pointed out by several authors, this is a technique that confers additional advantages for the diagnosis, for instance, the stray-flux is more immune to eventual harmonics introduced by load related problems, in comparison with other techniques such as current analysis since the rotor magneto-motive forces (MMF) or stray fluxes are not so influenced by oscillations or problems in the load [8], [13], [14]. Moreover, it has been proven, in the case of cage motors, that stray-flux-based methods are able to avoid some false indications (such as the influence of axial air ducts in the main sideband rotor fault harmonics) raising when using techniques relying on other quantities due to the spatial flux distribution [15]. Furthermore, in [8] it is demonstrated the potential of analyzing higher order fault-related harmonics of flux signals to avoid several sources of potential false diagnosis. This clear trend towards reliability aspects in the final diagnosis demonstrates the real need in the industry to count on reliable schemes able to effectively diagnose faults that commonly occur in electric motors, specially at incipient stages. Recent investigations have shown that the analysis of the stray flux under starting is a valuable tool to determine the condition of the rotor both in cage motors [16] and even in WRIM [11]. If these were not enough, some motor manufacturers are installing embedded flux sensors during the manufacturing process [17][18], a fact that may stimulate the potential massive extrapolation of this technique to the industrial context. Unfortunately, despite some recent works have explored the analysis of stray fluxes under starting to detect winding asymmetries in WRIM, they rely on the qualitative analysis of lower sideband harmonics, the evolutions of which may be interfered (at least partially) by other non-fault related problems.

The main contribution of this paper is a novel methodology for the detection and severity quantification of rotor asymmetries in WRIM by tracking multiple low and high order fault-related harmonics in the stray flux signals captured during the startup transient. It is shown that by means of a feed-forward neural network (FFNN) whose inputs are based on the proposed fault indicator, it is possible to obtain a reliable and automated final diagnosis, without the necessary intervention of an expert user to identify the fault patterns and reach a diagnosis conclusion. Furthermore, the obtained results demonstrate that tracking multiple harmonics yields a higher reliability in the diagnosis, in comparison with methods that depend on a single component evolution which can be masked (partially or totally) by different possible non-fault related causes: load torque oscillations, noises, supply voltage fluctuations), as it was already shown for other quantities [19]. Experimental results for 3 different levels of rotor asymmetries in a 11 kW WRIM prove the low cost, sensitive, and reliable fault detection capability of the proposal.

II. Theoretical Background

A. Theoretical Fault-related Components.

In healthy conditions, the stator and rotor impedances in a WRIM are ideally symmetrically distributed, and the currents are balanced. In this case, the balanced three-phase current system produces a fundamental clockwise rotating magnetic field in the air-gap. This field induces a current in the rotor winding with a frequency proportional to the rotor slip s. Then, the rotor winding generates a clockwise field rotating at $s \cdot f$. When there exists a rotor damage, symmetry of the machine is lost, and in accordance to the Fortescue's Theorem, a reverse rotating magnetic field is produced in addition to the clockwise field due to the imbalance rotor currents, which give rise to a frequency component at $-s \cdot f$. Subsequently, producing the well-known lower sideband harmonic (LSH) appearing in the

radial external magnetic field and in the line current, given by $f \cdot (1 - 2 \cdot s)$. As reported in some investigations [20], [21], it is possible to associate with this anticlockwise field a negative-sequence current system with amplitude I_{ccw}, which is added to the positive-sequence current system with amplitude I_{cc}, causing a pulsating torque and a speed oscillation [20]. Furthermore, it is well known that this speed oscillation also generates an additional air-gap flux density component at $(1 + 2 \cdot s) \cdot f$ [22]. As a consequence, a set of new components at frequencies $(f_{ksr} = (1 \pm 2 \cdot k \cdot s) \cdot f)_{k=0,1,2,\ldots}$ appears in the spectrum of the stator currents and a set of new components at frequencies $(f_{krr} = \pm(1 + 2 \cdot k) \cdot s \cdot f)_{k=0,1,2,\ldots}$ appears in the spectrum of rotor currents, which are reflected in the external magnetic field [21], [23], [24]. In addition to these fault-related harmonics, reference [25] determines equation (1), which estimates the frequency components amplified in the rotor currents caused by the rotor asymmetry.

$$f_{asym} = \left[\frac{k}{p} \cdot (1 - s) \pm s\right] \cdot f \qquad (1)$$

where f=supply frequency; s=slip and k/p=1,3,5, …

B. Multiple harmonics tracking in the stray-flux under starting.

Some investigations as in [16], [20], [26], [27] have shown that under a direct-on-line starting of an induction motor, well-known fault related harmonics (which are slip dependent) follow particular trajectories (as the slip changes from 1 to near 0 during the startup) in the time-frequency maps resulting from the analysis of the stray flux signals. The identification of these trajectories is a reliable tool to diagnose the rotor winding condition since their presence is a robust evidence of the existence of the fault, even under no load conditions. Moreover, it has been shown that the presence of the fault yields amplitude increments of a diversity of fault components with different nature (axial/radial). Therefore, if the flux sensor is properly attached to the motor frame, both types of components can be tracked and, hence, more reliable the diagnosis will be, since it will rely on multiple fault components and not only on a single harmonic that can be masked by different factors.

The idea of the present work is, indeed, to take advantages of a wide range of harmonics amplified by the rotor asymmetry to enhance the diagnosis of this failure in WRIM. Fig. 1 shows the expected time-frequency evolutions under starting of the harmonics amplified in the event of rotor asymmetries. These harmonics are described next:

- *Radial components*: given by expression (1). These correspond to a family of harmonics amplified by the rotor winding asymmetry in WRIM [20], [25]. For each value of k/p, expression (1) yields a pair of fault harmonics that evolve toward their respective frequencies at steady-state that fall near the corresponding winding harmonic (3th, 5th, 7th…winding harmonic). More specifically, for each value of k/p, the frequency of one of the components (indirect component) falls to zero before ascending again toward its steady-state value (e.g., f·(3-4·s), f·(5-6·s), f·(7-8·s), etc.), while the frequency of the other component (direct component) increases directly from its initial value (f) to its steady-state value (e.g., f·(3-2·s), f·(5-4·s), f·(7-6·s), etc.).

- *Axial components*: these are mainly the low-frequency harmonics at $s \cdot f$ and $3 \cdot s \cdot f$. Their amplitude can also be amplified by other faults such as eccentricities, as reported in previous works [20], [23]. The frequency of the component $s \cdot f$ starts at f when the machine is connected and ends at near 0 at steady-state, while the frequency of the $3 \cdot s \cdot f$ component starts at $3 \cdot f$ and ends at near 0 Hz, as shown in Fig. 1.

- *Rotational frequency components*: components at $f \pm f_r$, which are amplified by eccentricities or, to a lesser extent, by misalignments or load problems. As reported by some authors, their amplitudes are also amplified when rotor asymmetries are present [28]. Both components change their frequencies from their initial value (f in both cases) toward their respective steady-state frequencies ($f+f_r$ or $f-f_r$, respectively), as shown in Fig. 1.

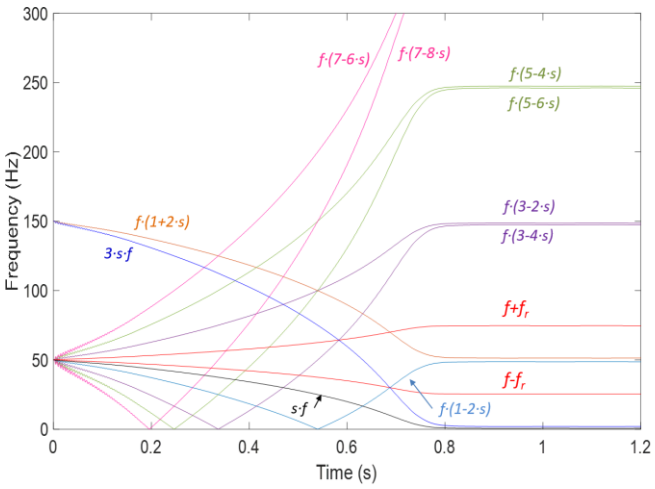

Fig. 1. Theoretical evolutions of the stray flux components amplified by rotor asymmetries during a simulated startup transient on an induction motor.

III. Proposed Methodology

The proposed methodology for the diagnosis of asymmetries in WRIM is based on the computation of indicators, which are related to the maximum energy density of multiple regions of the t-f map that are trespassed by relevant fault harmonics (shown in Fig.1) during their time-frequency evolution under starting. Since the method relies on multiple indicators, it is less likely to be influenced by non-fault related phenomena that may yield localized increments in specific regions of the t-f map, and

eventually lead to a false diagnosis. In this context, the time-frequency map shown in Fig. 1 enable a qualitative detection of the rotor winding asymmetry through the identification of the trajectories followed by different fault harmonics under starting. However, it becomes also necessary to propose indicators that enable to quantitatively determine the severity of the asymmetry. In this line, the advantage of the proposed methodology is that multiple indicators can be proposed, based on the increments experienced by the amplitudes of various harmonics. This fact confers a much higher accuracy and reliability for the diagnosis since a single indicator may be punctually altered by different phenomena or effects that are not related to the fault.

In accordance with the previous statements, several strategic time-frequency regions have been specified in the considered t-f maps (see the shadowed areas of Fig. 2: $\gamma_{A1},\gamma_{A2},\ldots,\gamma_{A7}$); a generic rotor asymmetry indicator is defined and computed at each one of the specified areas. The proposed indicator in each area (γ_A) relies on the computation of the maximum energy density in that area, as defined by (2) (where $En_{i,j}$ is the energy density at the (i, j) coordinate of the t-f map, t_0 and t_f are, respectively, the initial and final x-samples defining the considered t-f area and f_0 and f_f are, respectively, the initial and final y-samples defining the considered t-f area.

$$\gamma_A = Max(En_{i,j})_{i=t_0\ldots t_f;\ j=f_0\ldots f_f} \quad (2)$$

Following the abovementioned definitions, the proposed methodology (depicted in Fig. 2) is as follows:

1) Acquire the radial stray flux component (found around the WRIM frame) signal under startup transient by means of a proper waveform recorder and a flux sensor.
2) Obtain a time-frequency map of the radial stray flux signal by applying a suitable time-frequency decomposition mathematical tool; in this work it is used the STFT, due to its simplicity and clear visualization of fault components, in comparison with the Discrete tools [29].
3) Using (2), compute the proposed indicator (γ_A) in each region of interest for the different reference harmonics ($\gamma_{A1},\gamma_{A2},\ldots,\gamma_{A7}$). Since all the regions of interest are confined to a zone covered by the startup transient, it is proposed to isolate this transient by obtaining the upper envelope of the time-domain signal, and then setting a threshold value equal to the upper envelope maximum amplitude at steady state (which can be obtained from the last samples). This threshold value will be directly related to the end of the startup transient.
4) Classify the level of rotor asymmetry by evaluating the γ_A indicator. For the purposes of this paper, it is used a feed-forward neural network (FFNN) having two hidden layers with 4 and 6 neurons in each hidden layer, respectively. It is chosen a FFNN due to its simplicity, high performance as an automatic classifier, and the low burden required that its computation represents [30].

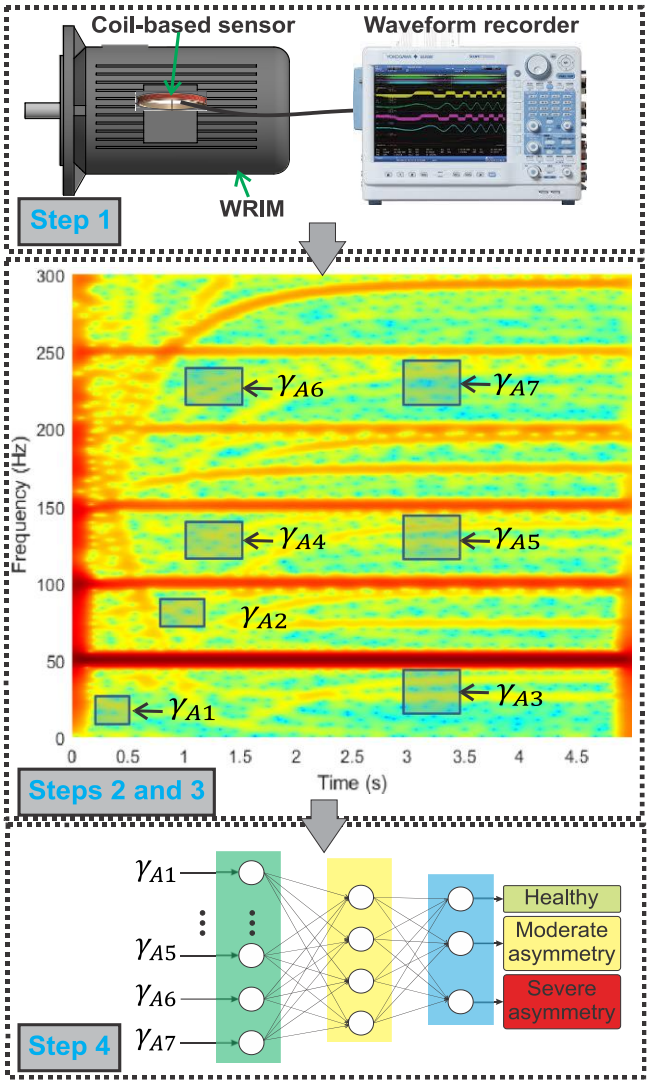

Fig. 2. Proposed methodology flow-up.

IV. Experimental Setup

Multiple experiments were developed using a laboratory 4P, 400V, 11kW WRIM with 24 rotor slots where the rotor winding coils were allocated. Under normal conditions, the machine was started by using an external three-phase starting rheostat that enabled to modify the speed-torque characteristic, obtaining a high starting torque while maintaining a low inrush current. Different severities of rotor winding asymmetry were forced by inserting an external resistor (R_{add}) in series with one of the rotor phases. This external resistor was based on a variable resistance that allowed to insert up to ten levels of resistance in series with the rotor phase: its maximum phase-to-phase resistance level was 11.6 Ω and the minimum 0.14 Ω. Fig. 3 shows a picture of the experimental test bench with all the elements commented above.

In each test, the WRIM was started direct-on-line by supplying the stator winding at 400 V. A coil-based flux sensor with 1000 turns (see geometric characteristics in Fig. 4) was connected to a waveform recorder (YOKOGAWA DL-850) that enabled to register the electromotive force (*emf*) induced

by the stray flux both under starting and under a certain time interval of the subsequent steady-state regime. The sampling rate used for the signal acquisition was 5 kHz. Different measurements were taken, considering several positions of the flux sensor. Fig. 3 shows one of the considered sensor positions, in which the captured stray flux is mainly radial and the corresponding fault components (radial) are more likely to be observed in the analyses. Three different fault severities are considered in this paper: healthy motor (inherent rotor asymmetry), moderate asymmetry (added resistance R_{add}=1.6 R_R, with R_R=rotor phase resistance) and high asymmetry (added resistance R_{add}=1.9 R_R). Tests were developed for the motor operating under no load, partial load and full load. However, in the paper only the no load results are depicted, because this is a more critical situation for detecting the fault related components in the flux signals, due to the reduced value of the slip *s*. Under this condition, the classical steady-state methods (e.g., MCSA or steady-state flux analysis) may have difficulties for detecting the $f\cdot(1\pm2\cdot s)$ components, as well as other high frequency harmonics (e.g., $f\cdot(5\text{-}6\cdot s)$ and $f\cdot(5\text{-}4\cdot s)$), since these may overlap with the supply frequency *f* or the corresponding winding harmonics (e.g., $5\cdot f$) due to the low slip value. The proposed starting transient based method avoids this problem, since the fault patterns are clearly present under starting regardless of the load level. Moreover, the load condition affects the duration of the startup yielding shorter startups at no load, which may make more difficult the detection of fault components' evolutions. This is another reason justifying the study of the no-load case. The waveform of the emf signal captured during one of the tests (sensor at the position shown in Fig. 3) is depicted in Fig.5.

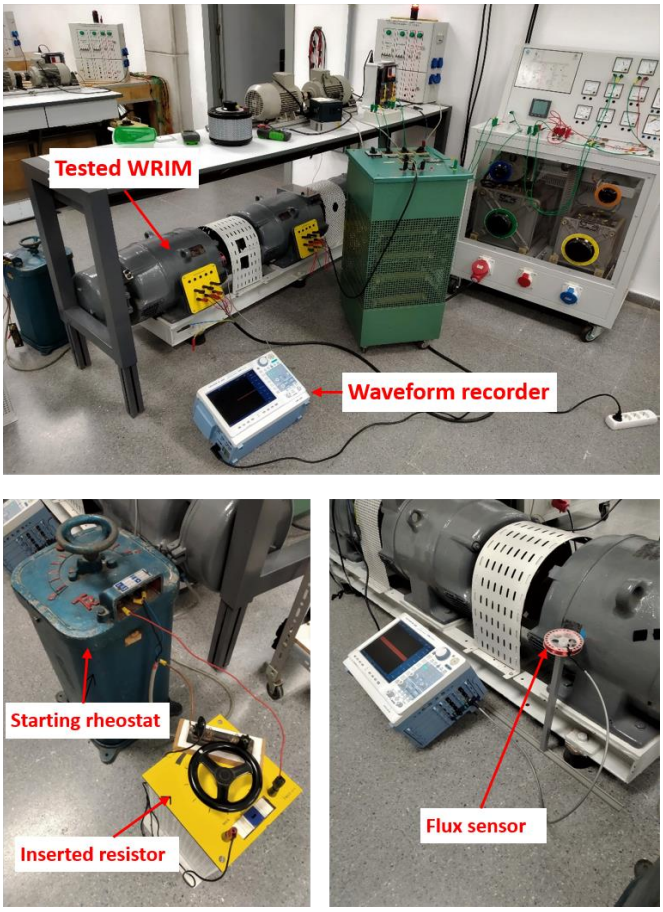

Fig. 3. Experimental test bench.

After the signals were registered, they were transferred to a PC and they were analyzed by applying an optimized Short Time Fourier Transform (STFT) using a self-built program implemented in Matlab, with a time window of 0.82 *s* and ratio between time and frequency resolution of the atom equal to 15 in order to track the evolution of the fault components. Additional information on the parameters used to compute the STFT can be found in [31]. The reason for selecting this specific time-frequency tool relies on its simplicity and availability in conventional mathematical packages. Finally, in order to train and validate the FFNN, a total of 150 signals were employed (50 tests per each condition state), each one corresponding to radial stray flux readings obtained under the starting. Out of the 50 signals captured for each condition, 20 of them were used for the FFNN training, while the remaining 30 signals were used for validation. Both the training and test procedures are carried out offline. The FFNN is trained through the Levenberg-Marquardt algorithm to identify a healthy (inherent asymmetry), a moderate asymmetry and a severe asymmetry. The FFNN final architecture has 7 inputs (7 reference harmonics), 4 and 6 neurons in the hidden layers, and 3 outputs (one per each WRIM condition state). The number of 4 and 6 neurons in the hidden layer is selected by trial and error in order to obtain the minimum overall classification error as suggested in [27]. The number of hidden layers is selected in order to get a good accuracy while retaining a small network size [28].

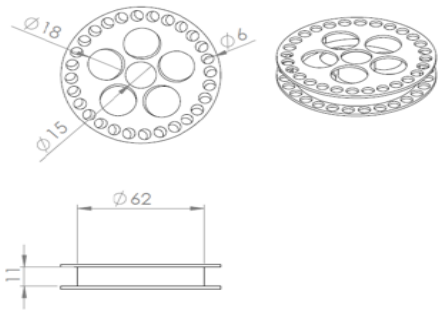

Fig. 4. Dimensions of the flux sensor.

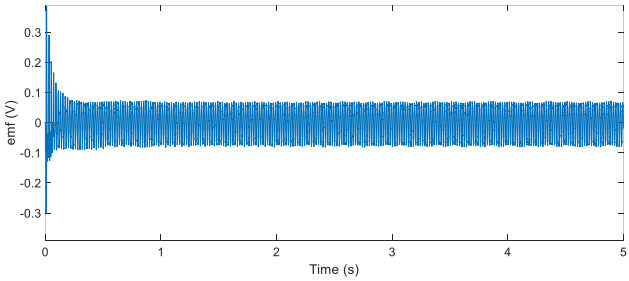

Fig. 5 Waveform of the induced emf signal in one of the tests under no load and for the sensor at Position C.

V. Results and Discussion

This section shows and discusses the results obtained during the experimentation by following the proposed methodology. Also, the evidences of high order fault-related harmonics found on the t-f maps are examined, and finally the FFNN overall classification effectiveness is disclosed.

Figs. 6-8 show the time-frequency analyses (range 0-300 Hz) of the *emf* signals that were registered under starting for the three aforementioned rotor winding asymmetry conditions, considering the sensor position shown in Fig. 3 (we will denote it by position C: the captured flux is primarily radial). In these figures, the color indicates the energy density in each point of the time-frequency map: red indicates the highest density while blue is for the lowest density. The graphs have been normalized so that the amplitudes are related to the maximum amplitude of that map.

Note the clear differences appearing between all three figures: at first sight, it is observed a much higher harmonic content (larger amplitudes for the fault components) when the fault severity is higher. This fact is a straight evidence of the presence of the anomaly. More specifically, a detailed analysis of these figures yields the following specific conclusions:

- Firstly, the evolutions of the main sideband harmonics related to the asymmetry (i.e., the LSH and the USH) are much clearer when the level of asymmetry is higher. This is due to the amplitude increment of these harmonics when the severity of the fault increases, as reported in previous works [11]. The V-shaped pattern caused by the starting evolution of f_{LSH} is particularly evident and is a clear indicator of the presence of the fault (see Fig. 8). Also, the descending evolution of the frequency of f_{USH} can be clearly observed in the maps and it is a good way to ratify the diagnostic provided by the f_{LSH}. In conclusion, the evolutions of these radial components are the most robust signatures of the existence of the rotor winding asymmetry.
- Second, a set of evolutions corresponding to higher order harmonics is also observable in the maps. These are the radial components given by (1) for k/p=3,5,7...Particularly evident are the fault harmonics $f_{3L}=f\cdot(3-4\cdot s)$ and $f_{3U}=f\cdot(3-2\cdot s)$, the evolutions of which end near the third winding harmonic ($3\cdot f$) and whose amplitudes are clearly incremented when the severity increases (compare these harmonics in Fig. 6 and Fig. 8). On the other hand, the evolutions of $f_{5L}=f\cdot(5-6\cdot s)$ and $f_{5U}=f\cdot(5-4\cdot s)$, are also clearly noticeable. Again, these harmonics have higher amplitudes as the level of asymmetry is increased (compare Fig. 6 and Fig. 8). Apart from these pairs of harmonics, other high-order harmonics given by (1) can be also partially observed in these time-frequency maps. In conclusion, the detection of all these evolutions are additional evidences of the existence of the asymmetry and can be used to reliably complement the information provided by the main sidebands.
- The evolutions of the axial components (especially, that of $s\cdot f$) are clearly discern. As commented for the previous components, the amplitudes of these harmonics also increase when the severity of the fault does. However, these components are not so noticeable as the radial ones. The reason is that, in this sensor position, the captured flux is primarily radial and the portion of axial flux that is captured is minor. In spite of this fact, the amplitudes increments are detectable (compare $s\cdot f$ in Figs. 6-8) and they can be used as complementary indicators of the presence of the asymmetry. Note that these axial components may be also amplified by eccentricities and other faults [20]. Hence, it is not advisable to rely only on them for the diagnostic. Note also that, for other sensor positions, these components will be more evident. Therefore, the combination of the information simultaneously obtained from different sensors may also be a good strategy for obtaining a more reliable diagnostic of the asymmetry.
- Finally, note that the components at the rotational frequency ($f\pm f_r$) also experience significant amplitude increments when the level of rotor winding asymmetry gets worse (compare these components in Figs. 6-8). This fact is in agreement with the conclusions of other authors [28] that stated these harmonics (usually linked with eccentricities or misalignments) are also amplified in the event of rotor asymmetries. Therefore, they constitute a fourth group of components that may serve to diagnose the presence of the asymmetry, in combination with the previous families.

Table I shows the results of the computation of the proposed indicator at the considered time-frequency regions of the map for the three different rotor winding asymmetry conditions, namely: healthy condition (inherent asymmetry of the rotor winding), moderate asymmetry and high asymmetry. It is worth to note the following facts derived from the observation of the results in Table I:

- The indicators relying on the time-frequency regions trespassed by the LSH and USH during the stating are suffering the largest increases when the fault is present. For the severe asymmetry case, the increment is higher than 18% for the LSH-based indicator.
- Significant increments are also obtained for the time-frequency region trespassed by the f-f_r component (increment near 15% for the case of severe asymmetry). This ratifies the fact that this component is significantly affected when the rotor asymmetry is present as stated in other works [28].
- The indicators relying on the fault harmonics ending near the third winding harmonic (f_{3L} & f_{3U}) also increase when the level of fault gets worse, reaching total increments of near 10% when the severe asymmetry is present.
- Finally, the indicators relying on the f_{5L} & f_{5U} harmonics also grow when the rotor winding asymmetry level is higher, reaching relevant increments (>10%) for the case of severe asymmetry.

All the previous indicators show gradual increases of their values as the level of asymmetry gets worse. This clearly proves that the level of failure can be correlated with the value of all proposed indicators.

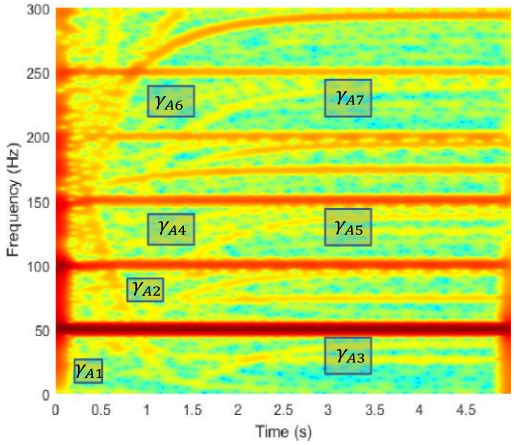

Fig. 6 Time-frequency analysis of the registered emf signal under starting for the motor with healthy rotor winding (inherent asymmetry) and considering the flux sensor at position C.

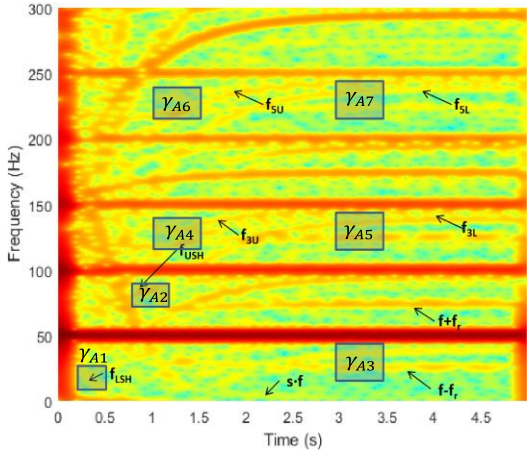

Fig. 7. Time-frequency analysis of the registered emf signal under starting for the motor with moderate rotor winding asymmetry and considering the flux sensor at position C.

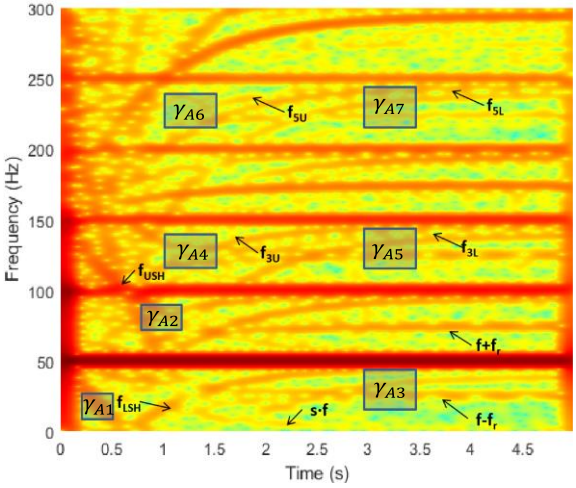

Fig. 8. Time-frequency analysis of the registered emf signal under starting for the motor with severe rotor winding asymmetry and considering the flux sensor at position C.

TABLE I
FAULT SEVERITY INDICATOR γ_A FOR THE DIFFERENT CONSIDERED AREAS OF THE TIME-FREQUENCY MAP

HEALTHY (INHERENT ASYMMETRY)				
γ_A index (Figs. 5-7)	**Reference harmonic**	**Time interval**	**Frequency interval**	**INDICATOR**
γ_{A1}	f_{LSH}	0.2 - 0.5 s	5-25 Hz	**-45.4**
γ_{A2}	f_{USH}	0.8 - 1.2 s	75-95 Hz	**-45.5**
γ_{A3}	$f-f_r$	3 - 3.5 s	20-40 Hz	**-47.6**
γ_{A4}	f_{3L} & f_{3U}	1 - 1.5 s	120-140 Hz	**-46.6**
γ_{A5}	f_{3L} & f_{3U}	3 - 3.5 s	120-145 Hz	**-44.5**
γ_{A6}	f_{5L} & f_{5U}	1 - 1.5 s	220-240 Hz	**-49.4**
γ_{A7}	f_{5L} & f_{5U}	3 - 3.5 s	220-245 Hz	**-47.8**
MODERATE ASYMMETRY				
γ_{A1}	f_{LSH}	0.2 - 0.5 s	5-25 Hz	**-41.8** (+7.9%)
γ_{A2}	f_{USH}	0.8 - 1.2 s	75-95 Hz	**-42.9** (+5.7%)
γ_{A3}	$f-f_r$	3 - 3.5 s	20-40 Hz	**-44.0** (+7.6%)
γ_{A4}	f_{3L} & f_{3U}	1 - 1.5 s	120-140 Hz	**-43.8** (+6.0%)
γ_{A5}	f_{3L} & f_{3U}	3 - 3.5 s	120-145 Hz	**-41.1** (+7.6%)
γ_{A6}	f_{5L} & f_{5U}	1 - 1.5 s	220-240 Hz	**-46.0** (+6.9%)
γ_{A7}	f_{5L} & f_{5U}	3 - 3.5 s	220-245 Hz	**-44.1** (+7.7%)
SEVERE ASYMMETRY				
γ_{A1}	f_{LSH}	0.2 - 0.5 s	5-25 Hz	**-34.2** (+18.2%)
γ_{A2}	f_{USH}	0.8 - 1.2 s	75-95 Hz	**-37.1** (+13.5%)
γ_{A3}	$f-f_r$	3 - 3.5 s	20-40 Hz	**-37.5** (+14.7%)
γ_{A4}	f_{3L} & f_{3U}	1 - 1.5 s	120-140 Hz	**-39.8** (+9.1%)
γ_{A5}	f_{3L} & f_{3U}	3 - 3.5 s	120-145 Hz	**-37.4** (+9.0%)
γ_{A6}	f_{5L} & f_{5U}	1 - 1.5 s	220-240 Hz	**-41.1** (+10.6%)
γ_{A7}	f_{5L} & f_{5U}	3 - 3.5 s	220-245 Hz	**-39.2** (+11.1%)

Furthermore, Fig. 9 illustrates the corresponding boxplots obtained for each of the proposed indices and each of the three different rotor winding asymmetry conditions. Note the relevance of considering the higher order harmonics. As it can be seen in Fig. 8, the f_{LSH} and f_{USH} indices exhibit a considerable overlap between healthy WRIM with inherent asymmetry and WRIM with moderate asymmetry. This condition may lead to inadequate final diagnosis as the main sideband harmonics are not consistent. On the other hand, if the higher order harmonics proposed in this work are evaluated, it is possible to appreciate a wide difference (in γ_A amplitudes) for all the case studies (see Fig. 9). This circumstance provides high reliability to the final diagnosis and potentially enables the use of an automatic classifier.

Table II shows the classification results as well as the effectiveness percentage of the proposed methodology. Correct classifications are located in the diagonal of Table II (highlighted in bold). In Table II, the first column represents the test data for the three different conditions. The first row represents the classification result of test data. The effectiveness, per condition state, is obtained through the calculation of the fault detection rate index (FDR) by dividing the number of correct classifications over the total number of samples. As shown in Table II, it can be concluded that the proposed methodology presents a 100% effectiveness when classifying for the three study cases analyzed.

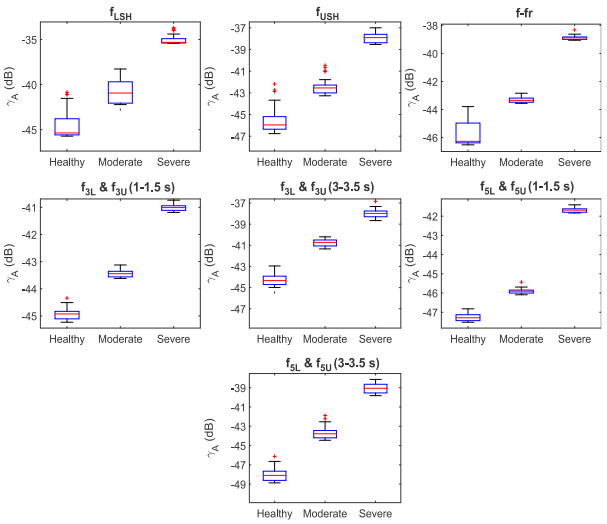

Fig. 9. Boxplots for all the seven evaluated harmonic reference and the three fault severity conditions.

VI. Conclusion

TABLE II
Effectiveness Percentage of the Proposed FFNN-based Method (Confusion Matrix)

	Healthy	Moderate asymmetry	Severe asymmetry	Effectiveness (%)
Healthy	**30**	0	0	100
Moderate asymmetry	0	**30**	0	100
Severe asymmetry	0	0	**30**	100

The present paper proposes a novel methodology for the diagnosis of rotor asymmetries in WRIM based on the time-frequency tracking on multiple harmonics, which are amplified by the presence of that failure. The method is based on a very recent trend relying on the analysis of the stray flux signals under starting: it has been proven that the tracking of the transient evolutions of the fault harmonics is a very reliable technique to diagnose the presence of the fault and determine its severity.

Unlike recent works that rely on a single harmonic (that may be masked or interfered by other phenomena), this paper proposes the use of multiple harmonics, a fact that provides additional accuracy and robustness for the diagnosis, as shown on the obtained results. In this regard, several fault severity indicators relying on strategic zones of the time-frequency maps resulting from the analyses of stray flux signals are proposed. These zones are trespassed by the considered fault harmonics during starting and their energy density is significantly increased when the fault severity gets worse. It is shown that all proposed indicators show relevant increments when the level of rotor winding asymmetry is increased.

Finally, the proposed method is automated by developing an FFNN-based system, which demonstrated an overall 100% effectiveness during the experiments when following the proposed methodology. This advanced feature confers potential for the implementation of the method in a real diagnostic system prototype relying on the use of this technique.

The underlying idea of the methodology proposed in this paper has shown very promising results regarding its recent extension to other machines such as synchronous motors [19], [32].

Acknowledgment

The authors would like to thank Consejo Nacional de Ciencia y Tecnologia, CONACyT under scholarship 65281.

References

[1] H. A. Toliyat and G. B. Kliman, *Handbook of Electric Motors*, vol. 120. CRC press, 2018.

[2] TECO-Westinghouse Motor Company, "Wound rotor motor technology." http://www.tecowestinghouse.com/PDF/woundrotor.pdf.

[3] All about circuits, "AC Motors," Chapter 13. Wound Rotor Induction Motors. https://www.allaboutcircuits.com/textbook/alternating-current/chpt-13/wound-rotor-induction-motors/.

[4] I. Tsoumas, "Analysis of the dynamic behaviour of the subsynchronous cascade drive and development of fault diagnosis methods," PhD Dissertation. Patras, Greece, 2007.

[5] J. Antonino-Daviu, A. Quijano-López, V. Climente-Alarcon, and C. Gar\'\in-Abellán, "Reliable detection of rotor winding asymmetries in wound rotor induction motors via integral current analysis," *IEEE Trans. Ind. Appl.*, vol. 53, no. 3, pp. 2040–2048, 2017.

[6] P. Tavner, L. Ran, J. Penman, and H. Sedding, *Condition monitoring of rotating electrical machines*, vol. 56. IET, 2008.

[7] Y. Gritli, C. Rossi, D. Casadei, F. Filippetti, and G. A. Capolino, "A Diagnostic Space Vector-Based Index for Rotor Electrical Fault Detection in Wound-Rotor Induction Machines under Speed Transient," *IEEE Trans. Ind. Electron.*, vol. 64, no. 5, pp. 3892–3902, 2017, doi: 10.1109/TIE.2017.2652389.

[8] S.-B. Lee, J. Shin, Y. Park, H. Kim, and J. Kim, "Reliable Flux based Detection of Induction Motor Rotor Faults from the 5th Rotor Rotational Frequency Sideband," *IEEE Trans. Ind. Electron.*, vol. 0046, no. c, pp. 1–1, 2020, doi: 10.1109/tie.2020.3016241.

[9] G. Mirzaeva, K. I. Saad, and M. G. Jahromi, "Comprehensive Diagnostics of Induction Motor Faults Based on Measurement of Space and Time Dependencies of Air Gap Flux," *IEEE Trans. Ind. Appl.*, vol. 53, no. 3, pp. 2657–2666, 2017, doi: 10.1109/TIA.2016.2628718.

[10] W. T. Thomson and I. Culbert, *Current Signature Analysis for Condition Monitoring of Cage Induction Motors: Industrial Application and Case Histories*. John Wiley & Sons, 2016.

[11] I. Zamudio-Ramirez, J. A. Antonino-Daviu, R. A. Osornio-Rios, R. De Jesus Romero-Troncoso, and H. Razik, "Detection of Winding Asymmetries in Wound-Rotor Induction Motors via Transient Analysis of the External Magnetic Field," *IEEE Trans. Ind. Electron.*, vol. 67, no. 6, pp. 5050–5059, 2020, doi: 10.1109/TIE.2019.2931274.

[12] M. E. Iglesias-Martinez, P. Fernandez De Cordoba, J. A. Antonino-Daviu, and J. Alberto Conejero, "Bispectrum Analysis of Stray Flux Signals for the Robust Detection of Winding Asymmetries in Wound Rotor Induction Motors," *ECCE 2020 - IEEE Energy Convers. Congr. Expo.*, pp. 4485–4490, 2020, doi: 10.1109/ECCE44975.2020.9235360.

[13] Y. Park, H. Choi, J. Shin, J. Park, S. Bin Lee, and H. Jo, "Airgap flux based detection and classification of induction motor rotor and load defects during the starting transient," *IEEE Trans. Ind. Electron.*, vol. 67, no. 12, pp. 10075–10084, 2020, doi: 10.1109/TIE.2019.2962470.

[14] K. N. Gyftakis, P. A. Panagiotou, and D. Spyrakis, "Recent Experiences with MCSA and Flux Condition Monitoring of Mechanical Faults in 6kV Induction Motors for Water Pumping Applications," in *Proceedings of the 2019 IEEE 12th International Symposium on Diagnostics for Electrical Machines, Power Electronics and Drives, SDEMPED 2019*, 2019, pp. 214–219, doi: 10.1109/DEMPED.2019.8864923.

[15] Y. Park *et al.*, "Stray flux monitoring for reliable detection of rotor faults under the influence of rotor axial air ducts," *IEEE Trans. Ind. Electron.*, vol. 66, no. 10, pp. 7561–7570, 2019, doi: 10.1109/TIE.2018.2880670.

[16] J. A. Ramirez-Nunez *et al.*, "Evaluation of the Detectability of Electromechanical Faults in Induction Motors Via Transient Analysis of the Stray Flux," *IEEE Trans. Ind. Appl.*, vol. 54, no. 5, pp. 4324–4332, 2018, doi: 10.1109/TIA.2018.2843371.

[17] Y. Park *et al.*, "Stray flux monitoring for reliable detection of rotor faults under the influence of rotor axial air ducts," *IEEE Trans. Ind. Electron.*, vol. 66, no. 10, pp. 7561–7570, 2019, doi: 10.1109/TIE.2018.2880670.

[18] ABB Motors, "ABB Ability ™ Smart Sensor," 2017. https://new.abb.com/motors-generators/service/advanced-services/smart-%0Asensor/smart-sensor-for-motors.

[19] J. Antonino-Daviu, V. Climente-Alarcon, I. Tsoumas, G. Georgoulas, and R. B. Perez, "Multi-harmonic tracking for diagnosis of rotor asymmetries in wound rotor induction motors," in *IECON Proceedings (Industrial Electronics Conference)*, 2013, pp. 5555–5560, doi: 10.1109/IECON.2013.6700043.

[20] A. Ceban, R. Pusca, and R. Romary, "Study of rotor faults in induction motors using external magnetic field analysis," *IEEE Trans. Ind. Electron.*, vol. 59, no. 5, pp. 2082–2093, 2012, doi: 10.1109/TIE.2011.2163285.

[21] Y. Gritli, L. Zarri, C. Rossi, F. Filippetti, G. A. Capolino, and D. Casadei, "Advanced diagnosis of electrical faults in wound-rotor induction machines," *IEEE Trans. Ind. Electron.*, vol. 60, no. 9, pp. 4012–4024, 2013, doi: 10.1109/TIE.2012.2236992.

[22] A. Bellini, F. Filippetti, G. Franceschini, C. Tassoni, and G. B. Kliman, "Quantitative evaluation of induction motor broken bars by means of electrical signature analysis," *IEEE Trans. Ind. Appl.*, vol. 37, no. 5, pp. 1248–1255, 2001, doi: 10.1109/28.952499.

[23] R. Romary, R. Pusca, J. P. Lecointe, and J. F. Brudny, "Electrical machines fault diagnosis by stray flux analysis," in *Proceedings - 2013 IEEE Workshop on Electrical Machines Design, Control and Diagnosis, WEMDCD 2013*, 2013, pp. 247–256, doi: 10.1109/WEMDCD.2013.6525184.

[24] F. Filippetti, G. Franceschini, C. Tassoni, and P. Vas, "AI techniques in induction machines diagnosis including the speed ripple effect," *IEEE Trans. Ind. Appl.*, vol. 34, no. 1, pp. 98–108, 1998, doi: 10.1109/28.658729.

[25] F. J. Vedreño Santos, "Diagnosis of electric induction machines in non-stationary regimes working in randomly changing conditions," Thesis Report, Universitat Politècnica de València, 2013.

[26] I. Zamudio-Ramirez, J. A. Antonino-Daviu, R. A. Osornio-Rios, R. De Jesus Romero-Troncoso, and H. Razik, "Detection of Winding Asymmetries in Wound-Rotor Induction Motors via Transient Analysis of the External Magnetic Field," *IEEE Trans. Ind. Electron.*, vol. 67, no. 6, pp. 5050–5059, 2020, doi: 10.1109/TIE.2019.2931274.

[27] H. Henao, C. Demian, and G. A. Capolino, "A frequency-domain detection of stator winding faults in induction machines using an external flux sensor," *IEEE Trans. Ind. Appl.*, vol. 39, no. 5, pp. 1272–1279, 2003, doi: 10.1109/TIA.2003.816531.

[28] K. N. Gyftakis, P. A. Panagiotou, and S. Bin Lee, "Generation of Mechanical Frequency Related Harmonics in the Stray Flux Spectra of Induction Motors Suffering from Rotor Electrical Faults," *IEEE Trans. Ind. Appl.*, vol. 56, no. 5, pp. 4796–4803, 2020, doi: 10.1109/TIA.2020.3002975.

[29] J. Pons-Llinares, J. A. Antonino-Daviu, M. Riera-Guasp, S. Bin Lee, T. J. Kang, and C. Yang, "Advanced induction motor rotor fault diagnosis via continuous and discrete time-frequency tools," *IEEE Trans. Ind. Electron.*, vol. 62, no. 3, pp. 1791–1802, 2015, doi: 10.1109/TIE.2014.2355816.

[30] M. Valtierra-Rodriguez, J. P. Amezquita-Sanchez, A. Garcia-Perez, and D. Camarena-Martinez, "Complete ensemble empirical mode decomposition on FPGA for condition monitoring of broken bars in induction motors," *Mathematics*, vol. 7, no. 9, p. 783, 2019, doi: 10.3390/math7090783.

[31] J. Pons-Llinares, M. Riera-Guasp, J. A. Antonino-Daviu, and T. G. Habetler, "Pursuing optimal electric machines transient diagnosis: The adaptive slope transform," *Mech. Syst. Signal Process.*, vol. 80, pp. 553–569, 2016, doi: 10.1016/j.ymssp.2016.05.003.

[32] M. F. Shaikh, J. Park, and S. Bin Lee, "A Non-Intrusive Leakage Flux Based Method for Detecting Rotor Faults in the Starting Transient of Salient Pole Synchronous Motors," *IEEE Trans. Energy Convers.*, vol. 36, no. 2, pp. 1262–1270, 2021, doi: 10.1109/TEC.2020.3021207.

BIOGRAPHIES

Israel Zamudio-Ramírez received his M.S. degree in mechatronic from the Autonomous University of Queretaro, Mexico, in 2019. He is currently working towards the Ph.D. degree at the Autonomous University of Queretaro with the Department of Mechatronics, Mexico and at the Universitat Politècnica de València with the Department of Electrical Engineering, Spain. His research interests include monitoring and diagnosis of electrical machines, embedded systems and hardware signal processing for engineering applications on FPGA.

Jose Antonino-Daviu (S'04, M'08, SM'12) received his M.S. and Ph. D degrees in Electrical Engineering, both from the Universitat Politècnica de València, in 2000 and 2006, respectively. Currently, he is Full Professor in the Department of Electrical Engineering of the mentioned University. He has been invited professor in Helsinki University of Technology (Finland) in 2005 and 2007, Michigan State University (USA) in 2010, Korea University (Korea) in 2014 and Université Claude Bernard Lyon 1 (France) in 2015. He is IEEE Senior Member since 2012 and he has published over 200 contributions. He is also Associate Editor of IEEE transactions on Industrial Informatics, IEEE Industrial Electronics Magazine and IEEE JESTIE. He is IEEE IAS Distinguished Lecturer for 2019-20. He was General Co-Chair of IEEE SDEMPED 2013. He received the Nagamori Award from Nagamori Foundation in Kyoto, Japan in 2018. In 2019, He got the SDEMPED Diagnostic Achievement Award for his contributions in electric motors condition monitoring.

Roque A. Osornio-Rios (M'10, SM'21) received the Ph.D. degree in mechatronics from the Autonomous University of Queretaro, Queretaro, Mexico, in 2007. Dr. Osornio-Rios is a National Researcher level 2 with the Mexican Council of Science and Technology, CONACYT. He is currently a Head Professor with the University of Queretaro, Mexico. He is advisor for more than 80 theses, and a coauthor of more than 100 technical papers published in international journals and conferences. His fields of interest include hardware signal processing and mechatronics. Dr. Osornio-Rios is fellow of the Mexican Academy of Engineering. Prof Osornio-Rios received the National Award in Investigation 2016 for Mexican Academy of Science. He is part of the editorial board of Journal and Scientific and Industrial Research.

Larisa Dunai (M´19), Associate Professor at Universitat Politecnica de Valencia (UPV), obtained her MSc degree in Electronic Engineering in 2003 from Technical University of Moldova. Afterwards, she joined that University as an Assistant professor at the Radio electronics and Telecommunications Department. In 2007 she started working as a researcher in the Research Center in Graphic Technology (CITG) of the UPV. In November 2008 she became Assistant professor of the Graphic Design Department. In 2010 obtained her PhD at UPV. In 2013 she received the MIT Innovators Award for Spain and in 2014 the Michael Richey Medal from Royal Institute of Navigation (UK).